Data-driven Predictive Voltage Control for Distributed Energy Storage in Active Distribution Networks

Yanda Huo, Peng Li, *Senior Member*, *IEEE*, *Member*, *CSEE*, Haoran Ji, *Senior Member*, *IEEE*, *Member*, *CSEE*, Hao Yu, *Senior Member*, *IEEE*, Jinli Zhao, *Member*, *IEEE*, Wei Xi, Jianzhong Wu, *Fellow*, *IEEE*, *Member*, *CSEE*, and Chengshan Wang, *Senior Member*, *IEEE*, *Member*, *CSEE*

***Abstract*—Integration of distributed energy storage (DES) is beneficial for mitigating voltage fluctuations in highly distributed generator (DG)-penetrated active distribution networks (ADNs). Based on an accurate physical model of ADN, conventional model-based methods can realize optimal control of DES. However, absence of network parameters and complex operational states of ADN poses challenges to model-based methods. This paper proposes a data-driven predictive voltage control method for DES. First, considering time-series constraints, a data-driven predictive control model is formulated for DES by using measurement data. Then, a data-driven coordination method is proposed for DES and DGs in each area. Through boundary information interaction, voltage mitigation effects can be improved by inter-area coordination control. Finally, control performance is tested on a modified IEEE 33-node test case. Case studies demonstrate that by fully utilizing multi-source data, the proposed predictive control method can effectively regulate DES and DGs to mitigate voltage violations.**

***Index Terms*—Distribution network, distributed energy storage (DES), distributed generators (DGs), data-driven, predictive voltage control.**

NOMENCLATURE

A. Sets

M	Set of areas in distribution networks.
R_m, L_m	Set of controllers of DES/DG in area m.

B. Indices

t	Indices of periods.
m	Indices of areas.
l, n	Indices of DES/DG.
z	Indices of data groups.

C. Variables

$\tilde{\boldsymbol{U}}[t], \boldsymbol{U}[t]$	Estimated /measurement voltage in period t.
$\tilde{\boldsymbol{U}}_N[t+\Delta t]$	Estimated value of nodal voltages from period $t+\Delta t$ to $t+N\Delta T_{\rm c}$.
$\boldsymbol{U}_N^{\rm ref}[t+\Delta t]$	Reference of nodal voltages from period $t+\Delta t$ to $t+N\Delta T_{\rm c}$.
$\hat{\boldsymbol{\Phi}}_{\rm pre}[t]$	Pseudo-Jacobian prediction matrix (PJPM) in period t.
$\hat{\phi}[t]$	Pseudo-Jacobi matrix (PJM) in period t.
$\hat{\phi}[t+n\Delta T_{\rm c}]$	Estimated value of PJM in period $t+n\Delta T_{\rm c}$.
$\Delta \boldsymbol{X}_N[t]$	Variation of the active power output of DES from period t to $t+N\Delta T_{\rm c}$.
$\Delta \boldsymbol{X}[t]$	Change of active power output of DES in period t.
$\boldsymbol{P}^{\rm DES}[t]$, $\boldsymbol{Q}^{\rm DES}[t]$	Active/reactive power of DES in period t.
$\rm SOC_0$, $\rm SOC_T$	State of charge (SOC) at initial/end of total control duration.
$\tilde{\boldsymbol{U}}_m[t], \boldsymbol{U}_m[t]$	Estimated /measurement voltage in area m in period t.
$\boldsymbol{P}_{m,l}^{\rm DES}[t]$, $\boldsymbol{Q}_{m,l}^{\rm DES}[t]$	Active/reactive power of DES l in area m in period t.
$\boldsymbol{P}_{m,r}^{\rm DG}[t]$, $\boldsymbol{Q}_{m,r}^{\rm DG}[t]$	Active/reactive power of DG r in area m in period t.
$\hat{\boldsymbol{\Phi}}_{m,r}^{\rm DG}[t]$, $\hat{\boldsymbol{\Phi}}_{m,l}^{\rm DES}[t]$	Estimated value of PJM of DG r/DES l in area m in period t.
$\boldsymbol{Y}_N^{\rm ref}$	Reference of modified control objective in area m.
$\tilde{\boldsymbol{Y}}_m$	Modified control objective in area m.
$\tilde{\boldsymbol{U}}_{{\rm vn},m}$	Estimated value of virtual voltage in area m.
$\tilde{P}_{{\rm vn},m}$	Estimated value of virtual active power injection in area m.
γ	Voltage deviation index.

D. Parameters

$\boldsymbol{U}^{\rm ref}$	Voltage reference of ADN.
$\Delta T_{\rm p}$	Prediction horizon.
$\Delta T_{\rm c}$	Prediction window.

Manuscript received May 3, 2022; revised September 14, 2022; accepted November 3, 2022. Date of online publication June 27, 2023; date of current version August 31, 2023. This work was supported by the National Key R&D Program of China (2020YFB0906000, 2020YFB0906001).

Y. D. Huo, P. Li, H. R. Ji (corresponding author, email: jihaoran@tju.edu.cn), H. Yu, J. L. Zhao and C. S. Wang are with School of Electrical and Information Engineering, Tianjin University, Tianjin 300072, China.

W. Xi is with Digital Power Grid Research Institute, China Southern Power Grid, Guangzhou 510630, China.

J. Z. Wu is with School of Engineering, Cardiff University, Cardiff CF24 3AA, U.K.

DOI: 10.17775/CSEEJPES.2022.02880

Δt	Control horizon.
T	Total control duration.
N	Number of steps of the prediction window.
T_{d}	The time interval between the time of historical data and period t.
α	Number of historical data groups for constructing the estimation sequence of $\hat{\phi}[t+n\Delta T_{\mathrm{c}}]$.
C^{DES}	Life-cycle degradation cost of DES.
S^{DES}	Capacity of DES.
S_{B}	Inverter capacity of DES.
$\mathrm{SOC}_{\max}$, $\mathrm{SOC}_{\min}$	Maximum/minimum value of the state of charge.
$P_{\max}$, $P_{\min}$	Maximum/minimum of active power outputs of DES.
N_m^{DG}, N_m^{DES}	Number of DG/DES in area m.
$\mu^{\mathrm{DES,p}}$, $\eta^{\mathrm{DES,p}}$, $\lambda^{\mathrm{DES,p}}$, $\rho^{\mathrm{DES,p}}$, $\delta\mu^{\mathrm{DES,q}}$, $\eta^{\mathrm{DES,q}}$, $\lambda^{\mathrm{DES,q}}$, $\rho^{\mathrm{DES,q}}$, μ^{DG}, η^{DG}, λ^{DG}, ρ^{DG}	Weight factors.
τ^{DES}	Power loss coefficient of DES.
ε	Charge/discharge threshold of DES.

I. Introduction

With high-share penetration of distributed generators (DGs) [1], operational mode has changed significantly in active distribution networks (ADNs) [2]. Rapid fluctuations in DGs pose significant challenges to secure operation of ADNs [3]. Conventional control devices for ADN, such as on-load tap changer and capacitor banks, discretely regulate voltage of distribution networks [4]. It is difficult for conventional devices to deal with frequent voltage fluctuations owing to slow response speed [5].

With application of energy storage technology, distributed energy storage (DES) has been widely used in ADN [6]. DES can be utilized to supply heavy load feeders, regulate voltage profile, and improve operational performance of ADNs [7]. Reference [8] proposed a voltage control scheme for DES in ADNs with large clustered DGs. Reference [9] proposed a distributed model predictive control strategy for DES to regulate voltage with high renewable energy penetration. In Reference [10], DG units, energy storage devices, and OLTC were regulated to improve voltage profile. To cope with time-series characteristics of DES, many studies have been carried out on the predictive voltage control for DES. A model predictive control-based method was proposed for hybrid energy storage regulation in Reference [11].

Inter-area coordinated control methods are also widely utilized for DES to assist areas with insufficient resources and achieve approximate optimal results. A revised alternating direction multiplier method was proposed in Reference [12] to guarantee convergence. Based on the master reactive power optimization model, distribution networks were coordinated to achieve global optimality in Reference [13]. In Reference [14], by decomposing into a set of independent subproblems, the centralized optimization problem was tractably solved. Demand response resources and energy storage were effectively coordinated in Reference [15].

The aforementioned control methods for DES are dependent on accurate and detailed physical models of ADNs. However, obtaining accurate model parameters is difficult for practical ADNs. In addition, frequent DG fluctuations may lead to voltage violations [16]. Model-based control approaches may not adapt well to various uncertainties in ADNs, including inaccuracy of network parameters and uncertainties caused by frequent variations in operation states. Therefore, model-based voltage control approaches for DESs face challenges in practical ADNs.

Owing to extensive application of measurement equipment [17] and accumulation of a large amount of operation data [18], data-driven approaches provide a promising approach for solving voltage control problems in ADNs [19]. There are two main categories of data-driven methods. First is based on machine learning. Through the centralized training process of reinforcement learning, data-driven control strategies for ADNs were obtained and executed in Reference [20]. Reference [21] developed a multistage adaptive robust optimization framework with reinforcement learning techniques to address uncertainties associated with high penetration of renewable energy. Reference [22] analyzed optimal power flow of ADNs utilizing a deep reinforcement learning approach. However, most reinforcement learning-based approaches may involve retraining when topology of ADNs changes, which may hinder its application.

The other is the online feedback-based control method [23], which establishes a data model without relying on training process [24], such as model-free adaptive control (MFAC) [25]. Reference [26] designed power system stabilizers based on MFAC and suppressed system oscillations. Reference [27] introduced the idea of prediction control in MFAC, achieving better control performance in time-series scenarios. In a previous study, an MFAC model for soft open point (SOP) was established, which realized adaptive control of SOP [28].

However, time-series characteristics of state of charge (SOC) should be considered in the DES control problem. To address this issue, this paper proposes a data-driven predictive control method for DES, as shown in Fig. 1. Considering time-series characteristics, a data-driven predictive control model is formulated to regulate DES strategies by using measurement data. Then, a data-driven coordination method is developed for DES and DGs in each area. Through boundary information interaction, data-driven control effects can be improved by inter-area coordination control. This paper makes two main contributions:

1) Considering time-series constraints of SOC, a rolling optimization framework is proposed for predictive voltage control of the DES. Without accurate network parameters, a data-driven predictive control model is formulated for DES with various data, including real-time measurements, prediction and historical information.

2) Then, a data-driven coordination method is proposed for DES and DGs in each area. The intra-area control model is

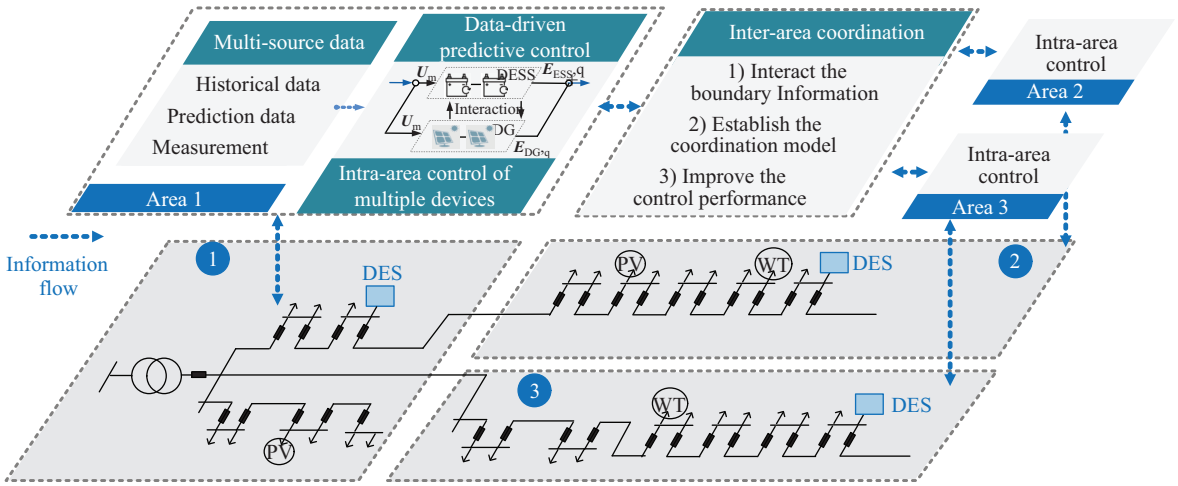

Fig. 1. Schematic of the data-driven predictive voltage control for DES.

built based on the superposition relationship of voltage control effect. Through boundary information interaction, data-driven control effects are improved by inter-area coordination control.

Organization of the rest of this paper is as follows: the adaptive control framework for DES is introduced in Section II, considering time-series constraints of SOC. In Section III, intra-area coordination of DES and DGs, and coordination of multiple areas are presented. In Section IV, case studies are conducted to demonstrate data-driven control effects, and Section V concludes the paper.

II. Data-driven Predictive Control of DES

Considering time-series constraints of SOC, a data-driven predictive control method is proposed for DES. The proposed method can dynamically optimize nodal voltages in real-time operations without accurate network parameters.

A. Framework of Data-driven Predictive Voltage Control

The proposed data-driven predictive voltage control framework is illustrated in Fig. 2.

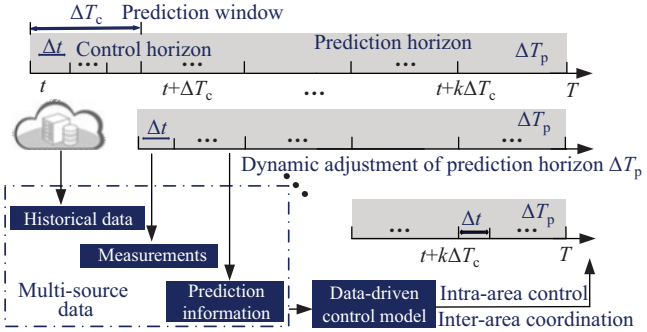

Fig. 2. Framework of the data-driven predictive control.

To realize time-series optimal control of the DES, three parts of data are utilized: prediction information, measurements and historical data. Prediction information of photovoltaics (PVs), wind turbines (WTs), and loads in total control duration are predicted based on operation curves [26]. Measurements can be acquired with measurement devices of ADNs. Historical data consists of nodal voltage and operational strategies of DES and DGs, which can be accumulated in previous days. In the process of data-driven predictive voltage control, strategies of DES and DGs can be equivalent to inputs of ADNs, whereas voltage measurements can be treated as outputs of ADNs.

As shown in Fig. 2, prediction horizon ΔT_p is divided into N segments. $N = \Delta T_\mathrm{p}/\Delta T_\mathrm{c}$, which represents number of prediction steps. Prediction information for PVs, WTs, and loads is updated in each prediction window ΔT_c. Operation strategies of the DES in ΔT_p are calculated based on real-time data in period t and predictive operation data during ΔT_p. Only the operation strategy in period t is implemented on the DES. Then, period was updated as $t = t + \Delta t$, and the above control process in period t was repeated until period t reached $t = t + \Delta T_\mathrm{c}$. Prediction horizon is updated to $\Delta T_\mathrm{p} = \Delta T_\mathrm{p} - \Delta T_\mathrm{c}$, and prediction information is also updated. The entire process is repeated until total control duration T is reached. By applying rolling optimization, operation strategies of the DES are dynamically adjusted for rapid response to DG and load fluctuations.

In the data-driven control process, decision variables to be solved include active power of DES, reactive power of DES and DGs. As for active power of DES, considering frequent charging/discharging will lower service life of DES, prediction window ΔT_c is set as 5 minutes. Active power strategies of DES considering time-series constraints are solved by commercial mathematical solver. However, as for reactive power of DES and DGs, control horizon Δt is set as 0.5 minutes. Solution of reactive power strategies is based on converter capacity constraints of DES and DGs, which can be solved by the gradient descent method to rapidly adapt to rapid fluctuations in DGs.

B. Modeling of Data-driven Predictive Voltage Control

To meet periodic energy balance requirement of DES in the regulation process of $\boldsymbol{P}_N^{\mathrm{DES}}[t]$, MPC is utilized with the data-driven method. In the 24-hour duration of ΔT_p, duration of ΔT_c is set as 5 minutes. Then $\boldsymbol{P}_N^{\mathrm{DES}}[t]$ can be solved by mathematical solvers. Specifically, the data-driven control

model of active power of DES is formulated as the following function:

1) Control Objective of DES

Minimum voltage violation and charging/discharging expense of DES by adjusting active power $\boldsymbol{P}^{\mathrm{DES}}[t]$ are adopted as objectives.

$$\begin{aligned} J(\boldsymbol{P}_N^{\mathrm{DES}}[t]) &= J_1 + J_2 + J_3 \\ J_1 &= \begin{pmatrix} \boldsymbol{U}_N^{\mathrm{ref}}[t+\Delta t] \\ -\tilde{\boldsymbol{U}}_N[t+\Delta t] \end{pmatrix}^{\mathrm{T}} \begin{pmatrix} \boldsymbol{U}_N^{\mathrm{ref}}[t+\Delta t] \\ -\tilde{\boldsymbol{U}}_N[t+\Delta t] \end{pmatrix} \\ J_2 &= C^{\mathrm{DES}} \sum_{i=1}^{N} |\boldsymbol{P}_i^{\mathrm{DES}}[t]| \\ J_3 &= \lambda^{\mathrm{DES,p}} (\Delta \boldsymbol{P}_N^{\mathrm{DES}}[t])^{\mathrm{T}} \Delta \boldsymbol{P}_N^{\mathrm{DES}}[t] \end{aligned} \tag{1}$$

where $\boldsymbol{U}_N^{\mathrm{ref}}[t+\Delta t]$ represents voltage reference from period $t+\Delta t$ to $t+N\Delta T_{\mathrm{c}}$. C^{DES} denotes life-cycle degradation cost of the DES. $\Delta \boldsymbol{P}_N^{\mathrm{DES}}[t] = (\Delta \boldsymbol{P}^{\mathrm{DES}}[t]^{\mathrm{T}}, \cdots, \Delta \boldsymbol{P}^{\mathrm{DES}}[t+(N-1)\Delta T_{\mathrm{c}}]^{\mathrm{T}})^{\mathrm{T}}$ denotes variation in charging/discharging power from period t to $t+N\Delta T_{\mathrm{c}}$. $\boldsymbol{P}^{\mathrm{DES}}[t]$ represents active power of DES in period t. $\tilde{\boldsymbol{U}}_N[t+\Delta t]$ denotes nodal voltages of ADNs from $t+\Delta t$ to $t+N\Delta T_{\mathrm{c}}$, which can be described as a time-series sequence: $\tilde{\boldsymbol{U}}_N[t+\Delta t] = (\tilde{\boldsymbol{U}}[t+\Delta t+\Delta T_{\mathrm{c}}]^{\mathrm{T}}, \cdots, \tilde{\boldsymbol{U}}[t+\Delta t+N\Delta T_{\mathrm{c}}]^{\mathrm{T}})^{\mathrm{T}}$.

2) Relationship between Voltage and Active Power of DES

To realize the control objective of DES, the time-series relationship between nodal voltages $\tilde{\boldsymbol{U}}_N[t+\Delta t]$ and active power of the DES need to be established. Based on dynamic linearization [30], $\tilde{\boldsymbol{U}}_N[t+\Delta t]$ can be estimated for each discrete period. The dynamic estimation model of nodal voltages is as follows:

$$\tilde{\boldsymbol{U}}_N[t+\Delta t] = \boldsymbol{E}[t]\boldsymbol{U}[t] + \hat{\boldsymbol{\Phi}}_{\mathrm{pre}}^{\mathrm{DES,p}}[t] \Delta \boldsymbol{P}_N^{\mathrm{DES}}[t] \tag{2}$$

where $\boldsymbol{E}[t]$ denotes unit vector. $\hat{\boldsymbol{\Phi}}_{\mathrm{pre}}^{\mathrm{DES,p}}[t]$ is PJPM in period t, which denotes the functional relationship between nodal voltages and charging/discharging power of DES.

3) Estimation of Pseudo-Jacobian Prediction Matrix

Calculated based on measurement data, PJPM characterizes the sensitivity relationship between voltage measurements and operational strategies of DES. The PJPM $\hat{\boldsymbol{\Phi}}_{\mathrm{pre}}^{\mathrm{DES,p}}[t]$ is defined as follows:

$$\hat{\boldsymbol{\Phi}}_{\mathrm{pre}}^{\mathrm{DES,p}} = \begin{bmatrix} \hat{\phi}^{\mathrm{DES,p}}[t] & \cdots & 0 \\ \vdots & \hat{\phi}^{\mathrm{DES,p}}[t+n\Delta T_{\mathrm{c}}] & \vdots \\ \hat{\phi}^{\mathrm{DES,p}}[t] & \cdots & \hat{\phi}^{\mathrm{DES,p}}[t+(N-1)\Delta T_{\mathrm{c}}] \end{bmatrix} \tag{3}$$

$\hat{\boldsymbol{\Phi}}_{\mathrm{pre}}^{\mathrm{DES,p}}[t]$ consists of two types of pseudo-Jacobian matrices, $\hat{\phi}^{\mathrm{DES,p}}[t]$ and $\hat{\phi}^{\mathrm{DES,p}}[t+n\Delta T_{\mathrm{c}}]$. To estimate $\hat{\boldsymbol{\Phi}}_{\mathrm{pre}}^{\mathrm{DES,p}}[t]$, the $\hat{\phi}^{\mathrm{DES,p}}[t]$ and $\hat{\phi}^{\mathrm{DES,p}}[t+n\Delta T_{\mathrm{c}}]$ must be calculated.

Located in the first column of $\hat{\boldsymbol{\Phi}}_{\mathrm{pre}}^{\mathrm{DES,p}}[t]$, $\hat{\phi}^{\mathrm{DES,p}}[t]$ is the pseudo-Jacobian matrix in period t, which can be calculated based on voltage measurement in period t. Calculation of $\hat{\boldsymbol{\Phi}}_{\mathrm{pre}}^{\mathrm{DES,p}}[t]$ is formulated as shown in (4) and (5).

$$\begin{aligned} \hat{\phi}^{\mathrm{DES,p}}[t] = \hat{\phi}^{\mathrm{DES,p}}[t-\Delta t] &+ \frac{\eta \Delta \boldsymbol{X}[t-\Delta t]}{\mu^{\mathrm{DES,p}} + \Delta \boldsymbol{X}[t-\Delta t]^2} \\ &(\Delta \boldsymbol{U}[t] - \hat{\phi}^{\mathrm{DES,p}}[t-\Delta t] \Delta \boldsymbol{X}[t-\Delta t]) \end{aligned} \tag{4}$$

$$\begin{aligned} \hat{\phi}^{\mathrm{DES,p}}[t] = \hat{\phi}^{\mathrm{DES,p}}[1], \\ \text{if } \hat{\phi}^{\mathrm{DES,p}}[t] \le \eta \text{ or } \Delta \boldsymbol{X}[t-\Delta t] \le \eta \\ \text{or } \operatorname{sign}(\hat{\phi}^{\mathrm{DES,p}}[t]) \ne \operatorname{sign}(\hat{\phi}^{\mathrm{DES,p}}[1]) \end{aligned} \tag{5}$$

where $\Delta \boldsymbol{X}[t-\Delta t] = \boldsymbol{P}^{\mathrm{DES}}[t-\Delta t] - \boldsymbol{P}^{\mathrm{DES}}[t-2\Delta t]$, $\Delta \boldsymbol{U}[t] = \boldsymbol{U}[t] - \boldsymbol{U}[t-\Delta t]$. The purpose of introducing (4) is to increase tracking ability of (3) [21].

The other element of $\hat{\boldsymbol{\Phi}}_{\mathrm{pre}}^{\mathrm{DES,p}}[t]$ can be expressed by the general formula $\hat{\phi}^{\mathrm{DES,p}}[t+n\Delta T_{\mathrm{c}}]$. It denotes the pseudo-Jacobian matrix in period $t+n\Delta T_{\mathrm{c}}$. $\hat{\phi}^{\mathrm{DES,p}}[t+n\Delta T_{\mathrm{c}}]$ can be estimated by a regression of a sequence of historical data groups, which are mainly accumulated in previous operational days. $\hat{\phi}^{\mathrm{DES,p}}[t+n\Delta T_{\mathrm{c}}]$ can be formulated as follows:

$$\hat{\phi}^{\mathrm{DES,p}}[t+n\Delta T_{\mathrm{c}}] = \sum_{z=1}^{\alpha} \theta_z[t] \hat{\phi}^{\mathrm{DES,p}}[t+n\Delta T_{\mathrm{c}} - zT_{\mathrm{d}}] \tag{6}$$

where $z = 1, 2, \cdots, \alpha$, denotes the number of historical data groups for constructing the estimation sequence. $\hat{\phi}^{\mathrm{DES,p}}[t+n\Delta T_{\mathrm{c}} - zT_{\mathrm{d}}]$ is the historical pseudo-Jacobian matrix calculated from historical data at $t+n\Delta T_{\mathrm{c}} - zT_{\mathrm{d}}$. $\theta_z[t]$ is the regression coefficient in period t.

To determine value of $\theta_z[t]$, a regression vector is defined as $\boldsymbol{\theta}[t] = (\theta_1[t], \cdots \theta_z[t], \cdots, \theta_\alpha[t])^{\mathrm{T}}$. $\boldsymbol{\theta}[t]$ can be calculated as follows:

$$\begin{aligned} \boldsymbol{\theta}[t] = \boldsymbol{\theta}[t-\Delta t] &+ \frac{\hat{\boldsymbol{\varphi}}[t-\Delta t]}{\delta + \| \hat{\boldsymbol{\varphi}}[t-\Delta t] \|^2} (\hat{\phi}[t] \\ &- \hat{\boldsymbol{\varphi}}^{\mathrm{T}}[t-\Delta t] \boldsymbol{\theta}[t-\Delta t]) \end{aligned} \tag{7}$$

where $\hat{\boldsymbol{\varphi}}[t-\Delta t] = (\hat{\phi}[t+n\Delta T_{\mathrm{c}} - T_{\mathrm{d}}], \cdots, \hat{\phi}[t+n\Delta T_{\mathrm{c}} - \alpha T_{\mathrm{d}}])^{\mathrm{T}}$, denotes a matrix consisting of pseudo-Jacobian matrices calculated from the historical data set.

4) Operational Constraints of DES

SOC constraint of DES within a prediction window ΔT_{c} is described as follows.

$$\begin{aligned} &\frac{\boldsymbol{S}^{\mathrm{DES}}}{\Delta T_{\mathrm{c}}} (\mathrm{SOC}_0 - \mathrm{SOC}_{\min}) - N \boldsymbol{P}^{\mathrm{DES}}[t] \\ &\le \begin{bmatrix} \Delta \boldsymbol{P}^{\mathrm{DES}}[t-\Delta t+\Delta T_{\mathrm{c}}] \\ \vdots \\ N\Delta \boldsymbol{P}^{\mathrm{DES}}[t-\Delta t+\Delta T_{\mathrm{c}}] + \\ (N-1)\Delta \boldsymbol{P}^{\mathrm{DES}}[t-\Delta t+2\Delta T_{\mathrm{c}}] + \\ \cdots + \Delta \boldsymbol{P}^{\mathrm{DES}}[t-\Delta t+N\Delta T_{\mathrm{c}}] \end{bmatrix} \\ &\le \frac{\boldsymbol{S}^{\mathrm{DES}}}{\Delta T_{\mathrm{c}}} (\mathrm{SOC}_{\max} - \mathrm{SOC}_0) - N \boldsymbol{P}^{\mathrm{DES}}[t] \end{aligned} \tag{8}$$

$$\mathrm{SOC}_0 = \mathrm{SOC}_T \tag{9}$$

where $\Delta \boldsymbol{P}^{\mathrm{DES}}[t-\Delta t+N\Delta T_{\mathrm{c}}] = \boldsymbol{P}^{\mathrm{DES}}[t-\Delta t+N\Delta T_{\mathrm{c}}] - \boldsymbol{P}^{\mathrm{DES}}[t-2\Delta t+N\Delta T_{\mathrm{c}}]$ denotes variation in the charging/discharging power in period $t-\Delta t+N\Delta T_{\mathrm{c}}$. Limits of charging/discharging power of DES are constrained as shown in the following equations.

$$(\boldsymbol{P}^{\mathrm{DES}}[t+n\Delta T_{\mathrm{c}}])^2 + (\boldsymbol{Q}^{\mathrm{DES}}[t+n\Delta T_{\mathrm{c}}])^2 \le \boldsymbol{S}_{\mathrm{B}}^2 \tag{10}$$

$$\boldsymbol{P}_{\min} \le \boldsymbol{P}^{\mathrm{DES}}[t+n\Delta T_{\mathrm{c}}] \le \boldsymbol{P}_{\max} \tag{11}$$

As frequent charging/discharging will lower service life of the DES, the following constraints should be added.

$$\boldsymbol{P}^{\mathrm{DES}}[t] = \begin{cases} \boldsymbol{0}, & \text{if } \operatorname{sign}(\boldsymbol{P}^{\mathrm{DES}}[t-\Delta t]) \\ & \neq \operatorname{sign}(\boldsymbol{P}^{\mathrm{DES}}[t-\Delta t]+\Delta \boldsymbol{X}[t]), \\ \boldsymbol{0}, & \text{if } |\Delta \boldsymbol{X}[t]| < \varepsilon \\ \boldsymbol{P}^{\mathrm{DES}}[t-\Delta t]+\tau^{\mathrm{DES}}\Delta \boldsymbol{P}^{\mathrm{DES}}[t], & \text{otherwise} \end{cases} \tag{12}$$

Constraint (12) limits fluctuation of DES charging and discharging power, which can decrease number of charge/discharge cycles.

Through this data-driven modeling, a predictive voltage control model is summarized as follows.

$$\begin{aligned} &\min f = J(\boldsymbol{P}_N^{\mathrm{DES}}[t]) \\ &\text{s.t. (2), (8)–(12)} \end{aligned} \tag{13}$$

The data-driven predictive voltage control model of DES active power is established by objective function (1) and SOC constraint of DES (8)–(11). Mathematical essence of the model is a quadratic programming model with constraints that can be solved by mathematical solver CVX.

III. Data-driven Coordinated Control

To efficiently realize decentralized voltage control, distribution networks can be divided into multiple areas according to regulation range [31]. To avoid operational conflicts caused by uncoordinated regulation among devices such as DGs and DES, a data-driven coordination method is proposed in each area. In addition, to realize approximate optimal control, inter-area coordination is also considered in this section.

A. Intra-area Control of Multiple Devices

With the data-driven predictive voltage control method in Section II, active power of DES can be calculated. Reactive power of DES can be coordinated with reactive power provided by residual capacity of DG inverter. As the voltage control model is dynamically linearized at each control period [21], a superposition relationship of voltage control effect exists between reactive power of DES and DGs. The control relationship between reactive power of DES and DGs is shown in Fig. 3.

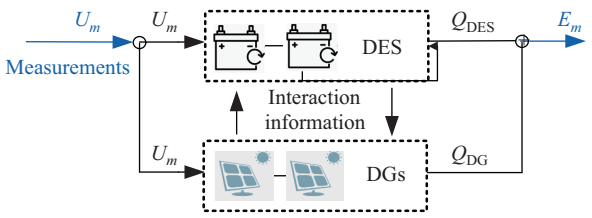

Fig. 3. Relationship between reactive power of DES and DGs.

As shown in Fig. 3, DES and DGs interact with intra-area information at each control period, including the pseudo-Jacobian matrices and reactive power of each other. The objective functions of the voltage control of the DES and DG are formulated as (14) and (15).

$$\begin{aligned} J(\boldsymbol{Q}_{m,r}^{\mathrm{DG}}[t]) = &\min(\|\boldsymbol{U}^{\mathrm{ref}} - \tilde{\boldsymbol{U}}_m[t+\Delta t]\|_2^2) \\ &+ \lambda^{\mathrm{DG}}\|\boldsymbol{Q}_{m,r}^{\mathrm{DG}}[t] - \boldsymbol{Q}_{m,r}^{\mathrm{DG}}[t-\Delta t]\|_2^2 \end{aligned} \tag{14}$$

$$\begin{aligned} J(\boldsymbol{Q}_{m,l}^{\mathrm{DES}}[t]) = &\min(\|\boldsymbol{U}^{\mathrm{ref}} - \tilde{\boldsymbol{U}}_m[t+\Delta t]\|_2^2 \\ &+ \lambda^{\mathrm{DES,q}}\|\boldsymbol{Q}_{m,l}^{\mathrm{DES}}[t] - \boldsymbol{Q}_{m,l}^{\mathrm{DES}}[t-\Delta t]\|_2^2) \end{aligned} \tag{15}$$

Considering the superposition relationship of voltage control effects between reactive power of DES and DGs, estimated value of $\tilde{\boldsymbol{U}}_m[t+\Delta t]$ is modified as follows:

$$\begin{aligned} \tilde{\boldsymbol{U}}_m[t+\Delta t] = &\boldsymbol{U}_m[t] + \sum_{r=1}^{N_m^{\mathrm{DG}}} \hat{\boldsymbol{\Phi}}_{m,r}^{\mathrm{DG,q}}[t] * \Delta \boldsymbol{Q}_{m,r}^{\mathrm{DG,q}}[t] \\ &+ \sum_{l=1}^{N_m^{\mathrm{DES}}} \hat{\boldsymbol{\Phi}}_{m,l}^{\mathrm{DES,q}}[t] * \Delta \boldsymbol{Q}_{m,l}^{\mathrm{DES,q}}[t] \\ &+ \sum_{l=1}^{N_m^{\mathrm{DES}}} \hat{\phi}_{m,l}^{\mathrm{DES,p}}[t] * \Delta \boldsymbol{P}_{m,l}^{\mathrm{DES}}[t] \end{aligned} \tag{16}$$

where $\Delta \boldsymbol{Q}_{m,r}^{\mathrm{DG}}[t] = \boldsymbol{Q}_{m,r}^{\mathrm{DG}}[t] - \boldsymbol{Q}_{m,r}^{\mathrm{DG}}[t-\Delta t]$. $\Delta \boldsymbol{Q}_{m,l}^{\mathrm{DES}}[t] = \boldsymbol{Q}_{m,l}^{\mathrm{DES}}[t] - \boldsymbol{Q}_{m,l}^{\mathrm{DES}}[t-\Delta t]$. $\hat{\boldsymbol{\Phi}}_{m,r}^{\mathrm{DG,q}}[t]$ and $\hat{\boldsymbol{\Phi}}_{m,l}^{\mathrm{DES,q}}[t]$ denote the pseudo-Jacobian matrix of the DG and DES, respectively. The iterative calculations of $\hat{\boldsymbol{\Phi}}_{m,r}^{\mathrm{DG,q}}[t]$ and $\hat{\boldsymbol{\Phi}}_{m,l}^{\mathrm{DES,q}}[t]$ are:

$$\begin{aligned} \hat{\boldsymbol{\Phi}}_{m,r}^{\mathrm{DG}}[t] = &\hat{\boldsymbol{\Phi}}_{m,r}^{\mathrm{DG}}[t-\Delta t] + (\Delta \boldsymbol{U}_m[t] \\ &- \sum_{n=1}^{N_m^{\mathrm{DG}}} \hat{\boldsymbol{\Phi}}_{m,r}^{\mathrm{DG}}[t]\Delta \boldsymbol{Q}_{m,r}^{\mathrm{DG}}[t-\Delta t] - \sum_{l=1}^{N_m^{\mathrm{DES}}} \hat{\phi}_{m,l}^{\mathrm{DES,p}}[t]\Delta \boldsymbol{P}_{m,l}^{\mathrm{DES}}[t] \\ &- \sum_{l=1}^{N_m^{\mathrm{DES}}} \hat{\boldsymbol{\Phi}}_{m,l}^{\mathrm{DES}}[t]\Delta \boldsymbol{Q}_{m,l}^{\mathrm{DES}}[t-\Delta t]) \frac{\eta^{\mathrm{DG}}\Delta \boldsymbol{Q}_{m,r}^{\mathrm{DG}}[t-\Delta t]}{\mu^{\mathrm{DG}} + \|\Delta \boldsymbol{Q}_{m,r}^{\mathrm{DG}}[t-\Delta t]\|_2^2} \end{aligned} \tag{17}$$

$$\begin{aligned} \hat{\boldsymbol{\Phi}}_{m,l}^{\mathrm{DES}}[t] = &\hat{\boldsymbol{\Phi}}_{m,l}^{\mathrm{DES}}[t-\Delta t] + (\Delta \boldsymbol{U}_m[t] \\ &- \sum_{n=1}^{N_m^{\mathrm{DG}}} \hat{\boldsymbol{\Phi}}_{m,r}^{\mathrm{DG}}[t]\Delta \boldsymbol{Q}_{m,r}^{\mathrm{DG}}[t-\Delta t] - \sum_{l=1}^{N_m^{\mathrm{DES}}} \hat{\phi}_{m,l}^{\mathrm{DES,p}}[t]\Delta \boldsymbol{P}_{m,l}^{\mathrm{DES}}[t] \\ &- \sum_{l=1}^{N_m^{\mathrm{DES}}} \hat{\boldsymbol{\Phi}}_{m,l}^{\mathrm{DES}}[t]\Delta \boldsymbol{Q}_{m,l}^{\mathrm{DES}}[t-\Delta t])) \\ &\cdot \frac{\eta^{\mathrm{DES,q}}\Delta \boldsymbol{Q}_{m,l}^{\mathrm{DES}}[t-\Delta t]}{\mu^{\mathrm{DES,q}} + \|\Delta \boldsymbol{Q}_{m,l}^{\mathrm{DES}}[t-\Delta t]\|_2^2} \end{aligned} \tag{18}$$

Introducing (16) into (14)–(15), solution of reactive power of DGs and DES can be formulated as (19)–(20) based on gradient descent methods [23].

$$\begin{aligned} \boldsymbol{Q}_{m,r}^{\mathrm{DG}}[t] = &\boldsymbol{Q}_{m,r}^{\mathrm{DG}}[t-\Delta t] + (\boldsymbol{U}^{\mathrm{ref}} - \tilde{\boldsymbol{U}}_m[t] \\ &- \sum_{a=1,a\neq r}^{N_m^{\mathrm{DG}}} \hat{\boldsymbol{\Phi}}_{m,a}^{\mathrm{DG}}[t]\Delta \boldsymbol{Q}_{m,a}^{\mathrm{DG}}[t] - \sum_{l=1}^{N_m^{\mathrm{DES}}} \hat{\phi}_{m,l}^{\mathrm{DES,p}}[t]\Delta \boldsymbol{P}_{m,l}^{\mathrm{DES}}[t] \\ &- \sum_{l=1}^{N_m^{\mathrm{DES}}} \hat{\boldsymbol{\Phi}}_{m,l}^{\mathrm{DES}}[t]\Delta \boldsymbol{Q}_{m,l}^{\mathrm{DES}}[t-\Delta t] \frac{\rho^{\mathrm{DG}}\hat{\boldsymbol{\Phi}}_{m,n}^{\mathrm{DG}}[t]}{\lambda^{\mathrm{DG}} + \|\hat{\boldsymbol{\Phi}}_{m,n}^{\mathrm{DG}}[t]\|_2^2} \end{aligned} \tag{19}$$

$$\boldsymbol{Q}_{m,l}^{\mathrm{DES}}[t] = \boldsymbol{Q}_{m,l}^{\mathrm{DES}}[t-\Delta t] + (\boldsymbol{U}^{\mathrm{ref}} - \tilde{\boldsymbol{U}}_m[t]$$

$$- \sum_{r=1}^{N_m^{\mathrm{DG}}} \hat{\boldsymbol{\Phi}}_{m,r}^{\mathrm{DG}}[t] \Delta \boldsymbol{Q}_{m,r}^{\mathrm{DG}}[t] - \sum_{l=1}^{N_m^{\mathrm{DES}}} \hat{\phi}_{m,l}^{\mathrm{DES,p}}[t] * \Delta \boldsymbol{P}_{m,l}^{\mathrm{DES}}[t] - \sum_{b=1, b\neq l}^{N_m^{\mathrm{DES}}} \hat{\boldsymbol{\Phi}}_{m,b}^{\mathrm{DES}}[t] \Delta \boldsymbol{Q}_{m,b}^{\mathrm{DES}}[t-\Delta t]) \frac{\rho^{\mathrm{DES,q}} \hat{\boldsymbol{\Phi}}_{m,l}^{\mathrm{DES}}[t]}{\lambda^{\mathrm{DES,q}} + \|\hat{\boldsymbol{\Phi}}_{m,l}^{\mathrm{DES}}[t]\|_2^2} \tag{20}$$

Considering limits of inverter capacities, reactive power outputs are constrained by (21) and (22).

$$(\boldsymbol{Q}_{m,r}^{\mathrm{DG}}[t])^2 \leq (\boldsymbol{S}_{m,r}^{\mathrm{DG}})^2 - (\boldsymbol{P}_{m,r}^{\mathrm{DG}}[t])^2, m \in M, r \in R_m \tag{21}$$

$$(\boldsymbol{Q}_{m,l}^{\mathrm{DES}}[t])^2 \leq (\boldsymbol{S}_{m,l}^{\mathrm{DES}})^2 - (\boldsymbol{P}_{m,l}^{\mathrm{DES}}[t])^2, m \in M, l \in L_m \tag{22}$$

Maximum and minimum limits of reactive power outputs are constrained by (23) and (24).

$$\boldsymbol{Q}_{m,r}^{\mathrm{DG,min}} \leq \boldsymbol{Q}_{m,r}^{\mathrm{DG}}[t] \leq \boldsymbol{Q}_{m,r}^{\mathrm{DG,max}} \tag{23}$$

$$\boldsymbol{Q}_{m,l}^{\mathrm{DES,min}} \leq \boldsymbol{Q}_{m,l}^{\mathrm{DES}}[t] \leq \boldsymbol{Q}_{m,l}^{\mathrm{DES,max}} \tag{24}$$

B. Inter-area Coordinated Control

To assist areas with insufficient resources and achieve approximate optimal results, the inter-area coordinated control method is conducted as follows: 1) Boundary information of maximum/minimum voltage value and active power transmission value are interacted between each area as boundary information. 2) Virtual nodes are set up in each area based on boundary information. 3) To obtain approximate optimal voltage control results, voltages of virtual nodes are taken into account in the data-driven control objective function to realize intra-area coordinated control.

Taking area m as an example, $U_{\mathrm{vn},m}$ and $P_{\mathrm{vn},m}$ are information transferred to area m. Then, voltage of the virtual node is merged with objective function of area m. The objective function of DES charging/discharging power control is modified as follows:

$$\begin{aligned} J(\Delta \boldsymbol{P}_{m,N}^{\mathrm{DES}}[t]) &= J_{m,1} + J_{m,2} + J_{m,3} \\ J_{m,1} &= \begin{pmatrix} \boldsymbol{Y}_N^{\mathrm{ref}}[t+\Delta t] \\ -\tilde{\boldsymbol{Y}}_{m,N}[t+\Delta t] \end{pmatrix}^{\mathrm{T}} \begin{pmatrix} \boldsymbol{Y}_N^{\mathrm{ref}}[t+\Delta t] \\ -\tilde{\boldsymbol{Y}}_{m,N}[t+\Delta t] \end{pmatrix} \\ J_{m,2} &= C^{\mathrm{DES}} \sum_{i=1}^{N} |\boldsymbol{P}_{m,i}^{\mathrm{DES}}[t]| \\ J_{m,3} &= \lambda^{\mathrm{DES,p}} (\Delta \boldsymbol{P}_{m,N}^{\mathrm{DES}}[t])^{\mathrm{T}} \Delta \boldsymbol{P}_{m,N}^{\mathrm{DES}}[t] \end{aligned} \tag{25}$$

$$\tilde{\boldsymbol{Y}}_{m,N}[t+\Delta t] = \boldsymbol{E}[t] \boldsymbol{U}_m[t] + \hat{\boldsymbol{\Phi}}_{\mathrm{pre}}[t] \Delta \boldsymbol{P}_{m,N}^{\mathrm{DES}}[t] \tag{26}$$

Similarly, objective functions of reactive power control of DES and DGs are modified as (27)–(29).

$$J(\boldsymbol{Q}_{m,r}^{\mathrm{DG}}[t]) = \min(\|\boldsymbol{Y}^{\mathrm{ref}} - \tilde{\boldsymbol{Y}}_m[t+\Delta t]\|_2^2 + \lambda^{\mathrm{DG}} \|\boldsymbol{Q}_{m,r}^{\mathrm{DG}}[t] - \boldsymbol{Q}_{m,r}^{\mathrm{DG}}[t-\Delta t]\|_2^2) \tag{27}$$

$$J(\boldsymbol{Q}_{m,l}^{\mathrm{DES}}[t]) = \min(\|\boldsymbol{Y}^{\mathrm{ref}} - \tilde{\boldsymbol{Y}}_m[t+\Delta t]\|_2^2 + \lambda^{\mathrm{DES,q}} \|\boldsymbol{Q}_{m,l}^{\mathrm{DES}}[t] - \boldsymbol{Q}_{m,l}^{\mathrm{DES}}[t-\Delta t]\|_2^2) \tag{28}$$

$$\tilde{\boldsymbol{Y}}_m[t+\Delta t] = \boldsymbol{Y}_m[t] + \sum_{r=1}^{N_m^{\mathrm{DG}}} \hat{\boldsymbol{\Phi}}_{m,r}^{\mathrm{DG}}[t] \Delta \boldsymbol{Q}_{m,r}^{\mathrm{DG}}[t] + \sum_{l=1}^{N_m^{\mathrm{DES}}} \hat{\boldsymbol{\Phi}}_{m,l}^{\mathrm{DES}}[t] \Delta \boldsymbol{Q}_{m,l}^{\mathrm{DES}}[t] + \sum_{l=1}^{N_m^{\mathrm{DES}}} \hat{\phi}_{m,l}^{\mathrm{DES,p}}[t] \Delta \boldsymbol{P}_{m,l}^{\mathrm{DES}}[t] \tag{29}$$

Equation (25) can be calculated by the method described in Section II. (27)–(28) can be calculated using the method in Section III-A.

C. Implementation

The flowchart of the proposed data-driven predictive voltage control is shown in Fig. 4.

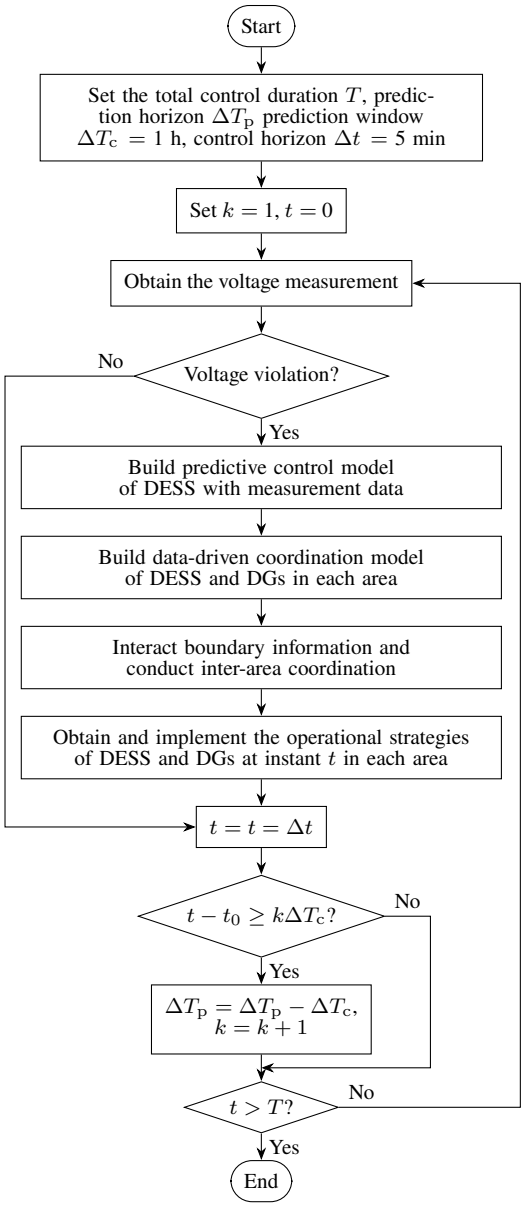

Fig. 4. Flowchart of the data-driven predictive voltage control.

First, the data-driven predictive voltage control model of the DES is formulated and solved based on multi-source data, including real-time measurements, prediction and historical information. Time-series operation constraints of DES are considered when calculating active power strategies of DES.

Then, considering the coupled voltage control effect of DES and DGs, an intra-area coordinated control model is

established. Reactive power of DES and DGs are coordinated to improve control performance.

In addition, virtual nodes are set up in each area to coordinate with adjacent areas, through interacting boundary information such as maximum/minimum voltage and active power transmission. To obtain approximate optimal voltage control results, inter-area coordinated control is conducted.

Note, to alleviate impact of control process on flexible operation of ADNs, change rates of DES and DGs are considered in the objective function. In addition, impact can be further reduced by introducing a penalty of voltage deviation into the objective function.

By utilizing the proposed coordinated control method, voltage deviation can be effectively suppressed, and approximated optimal results can be obtained.

IV. Case Studies

Case studies are conducted on the modified IEEE 33-node test system [29] in Fig. 5. The proposed data-driven predictive voltage control method is implemented in MATLAB R2016a, using an Intel Xeon CPU E5-1620 processor with 3.70 GHz and 32 GB of RAM.

A. Modified IEEE 33-node Test System

Three PVs are integrated to Nodes 4, 12, and 21 with capacities of 500.0 kWp. Four WTs are integrated to Nodes 9, 15, 24, and 29 with capacities of 500.0 kVA. Active power of the DGs reached almost 100% of peak demand. Fig. 6 shows daily operation curves of DG and load. In addition, three DESs are integrated into Nodes 18, 25, and 33, with a 4.0 MWh capacity each and a 500.0 kVA inverter capacity. Loss coefficient τ^{DES} of DES is set to 0.1.

B. Data-driven Control Results of DES

To ensure data-driven control convergence [27], weighting factor $\lambda^{\mathrm{DES,p}}$ is set as 10, and $\mu^{\mathrm{DES,p}}$ is set to 0.5. Other weighting factors, $\eta^{\mathrm{ESS,p}}$, $\rho^{\mathrm{ESS,p}}$, δ, $\mu^{\mathrm{ESS,q}}$, $\eta^{\mathrm{DES,q}}$, $\lambda^{\mathrm{DES,q}}$, $\rho^{\mathrm{DES,q}}$, μ^{DG}, η^{DG}, λ^{DG}, ρ^{DG} are all set to 1.0. Optimization horizon ΔT_c is set to one hour and control horizon Δt is set to five minutes. Three scenarios are set to verify data-driven control effects.

Scenario I: Obtain initial state of ADN with no control strategy for DG.

Scenario II: The data-driven predictive voltage control of DES is adopted with intra-area coordination of DES and DGs.

Scenario III: The inter-area coordinated control proposed in Section III is further conducted.

Taking the DES integrated into Node 33 as an example, operational strategies and the SOC of DES are shown in Fig. 7.

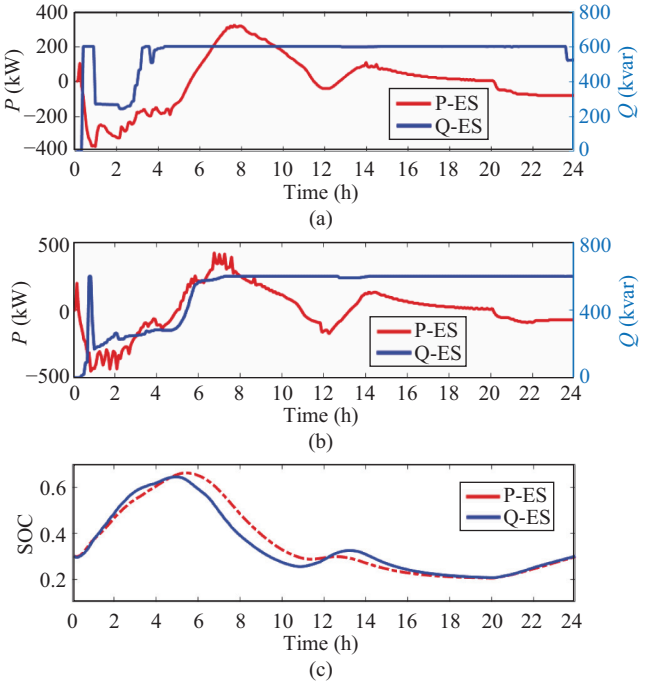

Fig. 7. Operational strategies of DES integrated to Node 33. (a) Operation strategy in Scenario II. (b) Operation strategies in Scenario III. (c) SOC of DES in Scenarios II and III.

In Fig. 7(a) and (b), red lines denote active power strategies of the DES. Negative value of active power indicates the DES is charging during this period. Blue lines represent reactive power strategies of DES. Similarly, negative value of reactive power denotes DES absorbs reactive power from ADN. Fig. 7(a)–(c) shows the data-driven predictive control method in Scenarios II and III can realize adaptive control of DES while satisfying the time-series constraint of the SOC. Fig. 8 illustrates daily voltage profiles of Node 33. Fig. 9 shows reactive power strategies of the WT integrated with Node 29.

During 0:00–4:00 am, active power generation of DGs is higher than load demand, which causes a voltage violation. DES charges and absorbs the reactive power. Conversely, during 2:00–6:00 pm, DGs fail to satisfy power demand. DES discharges and provides reactive power support. In addition, reactive power strategies of the DGs and DES are coordinated for a better voltage profile.

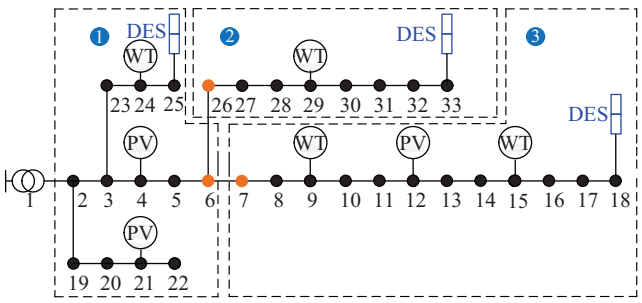

Fig. 5. Topology of the tested IEEE 33-node system.

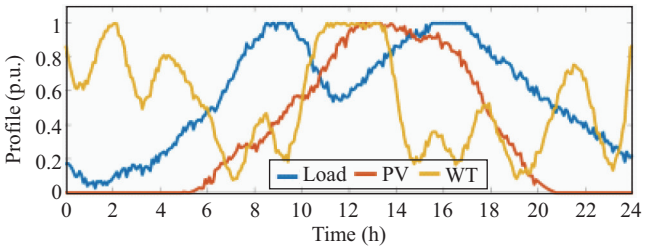

Fig. 6. Operational curves of DGs and loads.

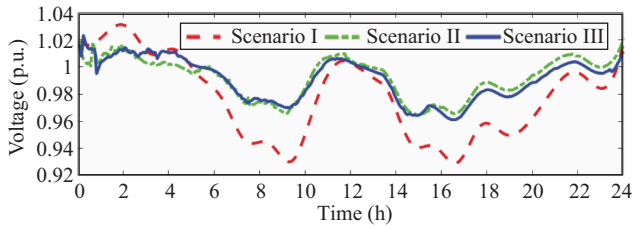

Fig. 8. Daily voltage profiles of Node 33.

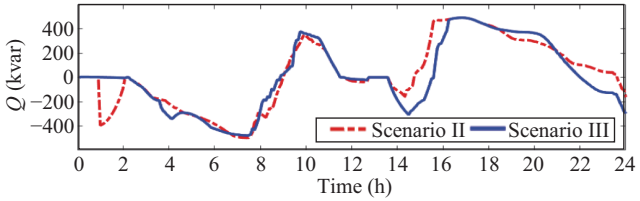

Fig. 9. Reactive power strategies of WT integrated to Node 29.

C. Analysis of Control Performance

Figure 10 shows a comparison of extreme voltages for the three scenarios. Power losses in the three scenarios are shown in Fig. 11. It shows the data-driven predictive control method in Scenario III has better effects in reducing voltage fluctuations and power losses.

The index of voltage deviation is defined to quantify control effects.

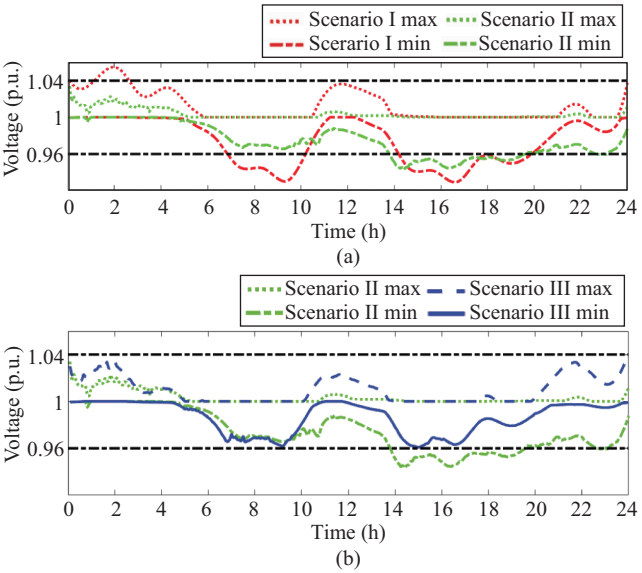

Fig. 10. Comparison of voltage profiles in Scenarios I, II and III. (a) Voltage profiles in Scenarios I and II. (b) Voltage profiles in Scenarios II and III.

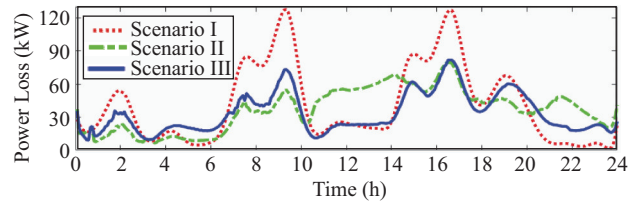

Fig. 11. Comparison of daily power losses.

$$\gamma = \frac{\sum_{t=1}^{T}\sum_{i=1}^{N}|U_{t,i}-1|}{T\cdot N} \tag{30}$$

where $U_{t,i}$ represents voltage of Node i in period t.

For example, at 4:00 p.m., control performance is illustrated in Fig. 12.

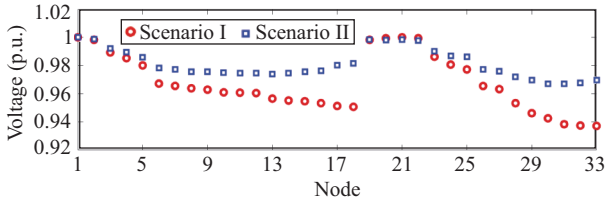

Fig. 12. Control performance at 4:00 pm.

It can be seen nodal voltage profiles of Scenario III are improved, and voltage deviation is regulated within 0.03. Scenario IV is further added for comparison as follows.

Scenario IV: The centralized control method based on the physical model is adopted [32].

Figure 13 shows comparison of voltage profiles from Scenarios III and IV. It shows control effects of Scenario III is approximate to Scenario IV. Table I lists operational results of the four scenarios.

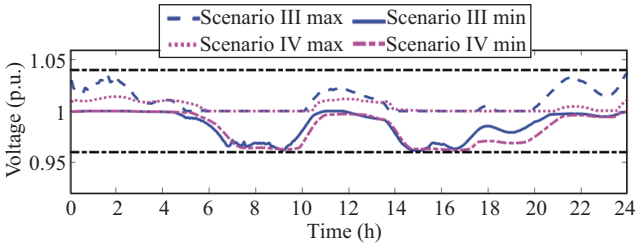

Fig. 13. Comparison of voltage profiles in Scenarios III and IV.

TABLE I
OPERATIONAL RESULTS OF THE TESTED SCENARIOS

Scenario	Minimum voltage (p.u.)	Maximum voltage (p.u.)	Index of voltage deviation (p.u.)	Power loss (kW·h)
I	0.9291	1.0547	0.0182	986.83
II	0.9431	1.0340	0.0121	888.92
III	0.9608	1.0341	0.0102	800.88
IV	0.9619	1.0140	0.0101	734.30

Compared to Scenario I, voltage deviation and network losses decrease by 33.52% and 9.92%, respectively, in Scenario II. In Scenario III, reductions are 43.96% and 18.84%, respectively. Voltage deviations are reduced in both Scenario II and Scenario III. With inter-area coordination in Scenario III, voltage control performance approximates the model-based centralized optimization in Scenario IV. To supplement second-level analysis, control horizon Δt is set as 0.5 minutes for quick response to frequent changes of DGs.

Scenario V: control horizon Δt is set as 0.5 minutes, the proposed control method is adopted.

As shown in Fig. 14 and Table II, with smaller control horizon Δt, the data-driven predictive voltage control method exhibits a faster response to voltage fluctuations, and control robustness is improved. However, due to frequent changes in

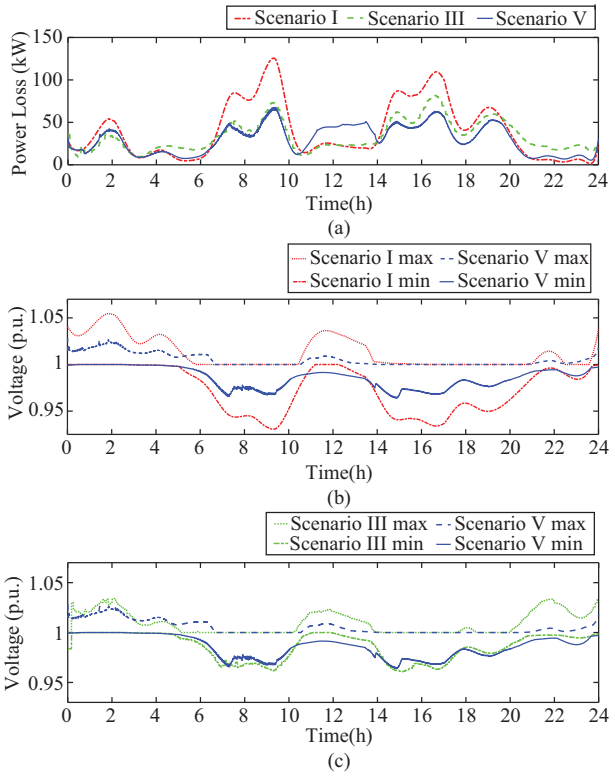

Fig. 14. Control performance comparison of 0.5-minutes control step. (a) Active power loss. (b) Voltage profiles of Scenarios I and V. (c) Voltage profiles Scenarios III and V.

operational strategies, power loss in Scenario V is increased by 5.98% compared with Scenario III. In addition, reduction of control horizon Δt will lead to heavier communication and computational burden. Thus, parameters of control horizon Δt should be chosen flexibly based on the practical operation situation.

D. Scalability Analysis

The modified IEEE 123-node test system is used to demenstrate scalability of the data-driven predictive control method, as shown in Fig. 15. Table III gives installation parameters of DG. Four DESs are integrated into Nodes 55, 95, 117 and 123 with the same parameters in Section IV-A.

With the same scenarios set in Section IV-B, Table IV shows operational results and Fig. 16 shows extreme system voltages. It can be seen the data-driven predictive control method is also applicable in large-scale ADNs.

In summary, the data-driven predictive voltage control method for DES effectively alleviates voltage violations and reduces power loss of ADNs. Through intra-area and inter-area coordination, approximate optimal results can also be achieved.

TABLE II
OPERATIONAL RESULTS OF THE THREE SCENARIOS

Scenario	Minimum voltage (p.u.)	Maximum voltage (p.u.)	Index of voltage deviation (p.u.)	Power loss (kW·h)
I	0.9291	1.0547	0.0182	986.83
III	0.9608	1.0341	0.0102	800.88
V	0.9640	1.0283	0.0093	848.81

TABLE III
INSTALLATION PARAMETERS OF DGS

Type	Node	Capacity/kVA (kWp)
WT	28, 92, 108	1000
PV	33, 42, 86, 97, 111, 116	500

TABLE IV
OPERATIONAL RESULTS OF TWO SCENARIOS

Scenario	Minimum voltage (p.u.)	Maximum voltage (p.u.)	Index of voltage deviation (p.u.)	Power loss (kW·h)
I	0.9114	1.0291	0.0308	1952.3
III	0.9764	1.0207	0.0047	1407.8

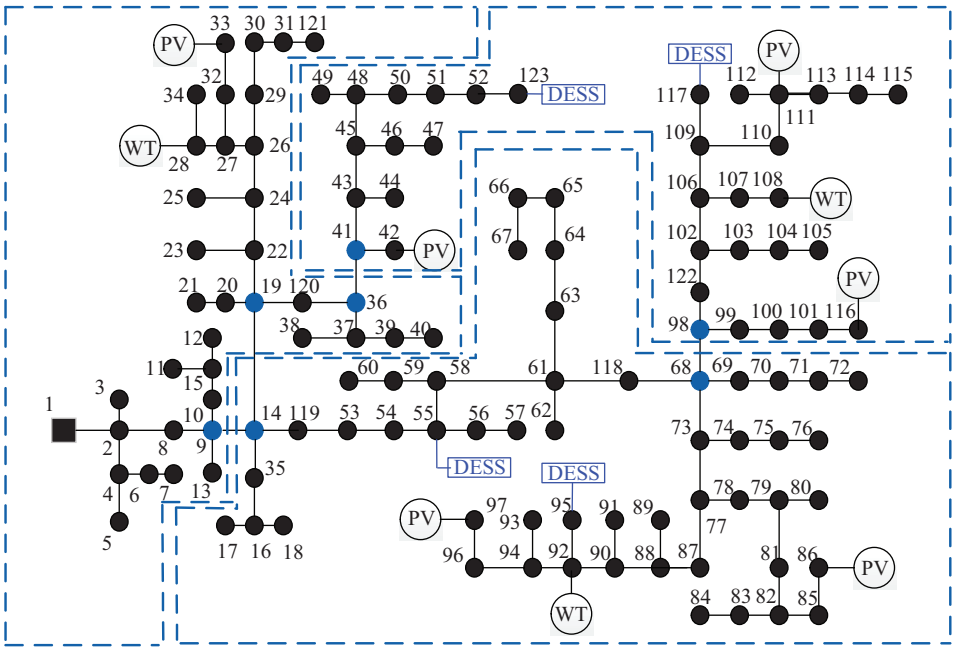

Fig. 15. Topology of the tested IEEE 123-node system.

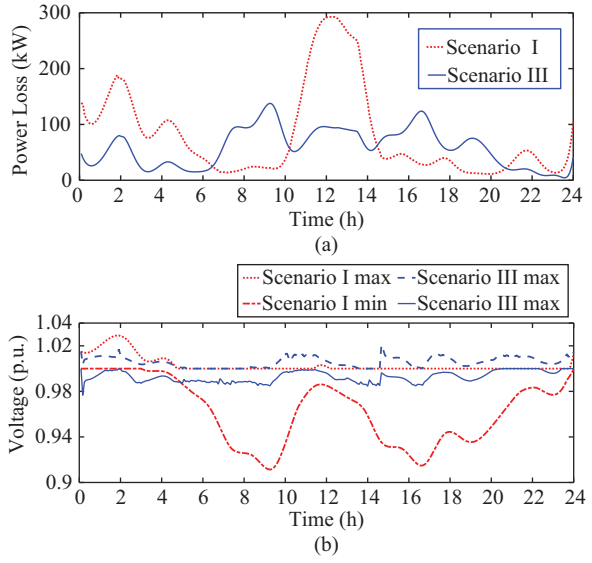

Fig. 16. Operational results of Scenarios I and III. (a) Active power loss. (b) Voltage profiles.

V. Conclusion

A data-driven predictive control method is proposed for DES, which is applicable without accurate network parameters. Based on measurement data, a rolling optimization framework can be utilized to dynamically determine operational strategies of DES with time-series constraints of SOC. In addition, to avoid operational conflicts caused by uncoordinated regulation among devices, a data-driven coordinated method is developed for DES and DGs in each area. The intra-area control model is formulated with the superposition relationship of voltage control effect. Through boundary information interaction, data-driven control performance is improved by inter-area coordination control. Case studies illustrate that by fully utilizing multi-source data, the proposed predictive control method can effectively regulate DES and DGs to mitigate voltage violations.

In future research, fusion of physical and data models can be considered. With precise modeling, physical models have accurate solutions. Inaccurate or absent parameters may affect performance of a physical model. Relying on a large amount of operational data, data-driven models can respond to state changes rapidly. Fusion of physical and data models can merge the advantages of both physical and data models, which is promising for further study.

References

[1] M. A. Ebrahim, F. Wadie, and M. A. Abd-Allah, "An algorithm for detection of fault, islanding, and power swings in DG-equipped radial distribution networks," *IEEE Systems Journal*, vol. 14, no. 3, pp. 3893–3903, Sep. 2020.

[2] S. X. Zhang, Y. C. Fang, H. Zhang, H. Z. Cheng, and X. Wang, "Maximum hosting capacity of photovoltaic generation in SOP-based power distribution network integrated with electric vehicles," *IEEE Transactions on Industrial Informatics*, vol. 18, no. 11, pp. 8213–8224, Nov. 2022.

[3] X. Q. Fu, "Statistical machine learning model for capacitor planning considering uncertainties in photovoltaic power," *Protection and Control of Modern Power Systems*, vol. 7, no. 1, pp. 5, Feb. 2022.

[4] J. Jian, P. Li, H. Yu, H. R. Ji, J. Ji, G. Y. Song, J. Y. Yan, J. Z. Wu, and C. S. Wang, "Multi-stage supply restoration of active distribution networks with SOP integration," *Sustainable Energy, Grids and Networks*, vol. 29, pp. 100562, Mar. 2022.

[5] F. Ding and B. Mather, "On distributed PV hosting capacity estimation, sensitivity study, and improvement," *IEEE Transactions on Sustainable Energy*, vol. 8, no. 3, pp. 1010–1020, Jul. 2017.

[6] H. Zhu, H. Li, G. J. Liu, Y. Ge, J. Shi, H. Li and N. Zhang, "Energy storage in high variable renewable energy penetration power systems: Technologies and applications," *CSEE Journal of Power and Energy Systems*, vol. 9, no. 6, pp. 2099–2108, Nov. 2023.

[7] S. S. Sami, M. Cheng, J. Z. Wu, and N. Jenkins, "A virtual energy storage system for voltage control of distribution networks," *CSEE Journal of Power and Energy Systems*, vol. 4, no. 2, pp. 146–154, Jun. 2018.

[8] P. F. Wang, D. H. Liang, J. L. Yi, P. F. Lyons, P. J. Davison, and P. C. Taylor, "Integrating electrical energy storage into coordinated voltage control schemes for distribution networks," *IEEE Transactions on Smart Grid*, vol. 5, no. 2, pp. 1018–1032, Mar. 2014.

[9] K. Meng, Z. Y. Dong, Z. Xu, and S. R. Weller, "Cooperation-driven distributed model predictive control for energy storage systems," *IEEE Transactions on Smart Grid*, vol. 6, no. 6, pp. 2583–2585, Nov. 2015.

[10] Y. F. Guo, Q. W. Wu, H. L. Gao, X. Y. Chen, J. Østergaard, and H. H. Xin, "MPC-Based coordinated voltage regulation for distribution networks with distributed generation and energy storage system," *IEEE Transactions on Sustainable Energy*, vol. 10, no. 4, pp. 1731–1739, Oct. 2019.

[11] X. B. Zhang, B. F. Wang, D. Gamage, and A. Ukil, "Model predictive and iterative learning control based hybrid control method for hybrid energy storage system," *IEEE Transactions on Sustainable Energy*, vol. 12, no. 4, pp. 2146–2158, Oct. 2021.

[12] S. Y. Li, W. C. Wu, and Y. Lin, "Robust data-driven and fully distributed Volt/VAR control for active distribution networks with multiple virtual power plants," *IEEE Transactions on Smart Grid*, vol. 13, no. 4, pp. 2627–2638, Jul. 2022.

[13] T. Ding, C. Li, C. Huang, Y. H. Yang, F. X. Li, and F. Blaabjerg, "A hierarchical modeling for reactive power optimization with joint transmission and distribution networks by curve fitting," *IEEE Systems Journal*, vol. 12, no. 3, pp. 2739–2748, Sep. 2018.

[14] F. Qi, M. Shahidehpour, F. S. Wen, Z. Y. Li, Y. B. He, and M. Y. Yan, "Decentralized privacy-preserving operation of multi-area integrated electricity and natural gas systems with renewable energy resources," *IEEE Transactions on Sustainable Energy*, vol. 11, no. 3, pp. 1785–1796, Jul. 2020.

[15] H. M. Yang, W. D. Shen, Q. Yu, J. P. Liu, Y. Z. Jiang, E. Ackom, and Z. Y. Dong, "Coordinated demand response of rail transit load and energy storage system considering driving comfort," *CSEE Journal of Power and Energy Systems*, vol. 6, no. 4, pp. 749–759, Dec. 2020.

[16] H. Di, L. Sun, and M. Ding, "Integrated planning of an active distribution network and DG integration in clusters considering a novel formulation for reliability assessment," *CSEE Journal of Power and Energy Systems*, vol. 9, no. 2, pp. 561–576, Mar. 2023.

[17] W. T. Zhang, D. Yang, and H. C. Wang, "Data-driven methods for predictive maintenance of industrial equipment: a survey," *IEEE Systems Journal*, vol. 13, no. 3, pp. 2213–2227, Sep. 2019.

[18] M. Yang, A. Bo, R. S. He, C. Huang, Z. F. Ma, Z. D. Zhong, J. H. Wang, L. Pei, Y. J. Li, and J. Li, "Machine-learning-based fast angle-of-arrival recognition for vehicular communications," *IEEE Transactions on Vehicular Technology*, vol. 70, no. 2, pp. 1592–1605, Feb. 2021.

[19] L. Q. Bai, Y. S. Xue, G. L. Xu, J. Dong, M. M. Olama, and T. Kuruganti, "A data-driven network optimisation approach to coordinated control of distributed photovoltaic systems and smart buildings in distribution systems," *IET Energy Systems Integration*, vol. 3, no. 3, pp. 285–294, Sep. 2021.

[20] D. Cao, J. B. Zhao, W. H. Hu, F. Ding, Q. Huang, Z. Chen, and F. Blaabjerg, "Data-driven multi-agent deep reinforcement learning for distribution system decentralized voltage control with high penetration of PVs," *IEEE Transactions on Smart Grid*, vol. 12, no. 5, pp. 4137–4150, Sep. 2021.

[21] N. Zhao and F. Q. You, "New York State's 100% renewable electricity transition planning under uncertainty using a data-driven multistage adaptive robust optimization approach with machine-learning," *Advances in Applied Energy*, vol. 2, pp. 100019, May 2021.

[22] D. Cao, W. H. Hu, X. Xu, Q. W. Wu, Q. Huang, Z. Chen, and F. Blaabjerg, "Deep reinforcement learning based approach for optimal power flow of distribution networks embedded with renewable energy

and storage devices," *Journal of Modern Power Systems and Clean Energy*, vol. 9, no. 5, pp. 1101–1110, Sep. 2021.
[23] T. Xu, W. C. Wu, Y. W. Hong, J. J. Yu and F. Z. Zhang, "Data-driven inverter-based Volt/VAr control for partially observable distribution networks," *CSEE Journal of Power and Energy Systems*, vol. 9, no. 2, pp. 548–560, Mar. 2023.
[24] Z. S. Hou and Y. M. Zhu, "Controller-dynamic-linearization-based model free adaptive control for discrete-time nonlinear systems," *IEEE Transactions on Industrial Informatics*, vol. 9, no. 4, pp. 2301–2309, Nov. 2013.
[25] Z. S. Hou and S. T. Jin, "Data-driven model-free adaptive control for a class of MIMO nonlinear discrete-time system," *IEEE Transactions on Neural Networks*, vol. 22, no. 12, pp. 2173–2188, Dec. 2011.
[26] Y. Guo, Z. S. Hou, S. D. Liu, and S. T. Jin, "Data-driven model-free adaptive predictive control for a class of MIMO nonlinear discrete-time systems with stability analysis," *IEEE Access*, vol. 7, pp. 102852–102866, Jul. 2019.
[27] S. X. Wang, J. S. Li, Z. S. Hou, Q. Y. Meng, and M. Li, "Composite model-free adaptive predictive control for wind power generation based on full wind speed," *CSEE Journal of Power and Energy Systems*, vol. 8, no. 6, pp. 1659–1669, Nov. 2022.
[28] Y. D. Huo, P. Li, H. R. Ji, J. Y. Yan, G. Y. Song, J. Z. Wu, and C. S. Wang, "Data-driven adaptive operation of soft open points in active distribution networks," *IEEE Transactions on Industrial Informatics*, vol. 17, no. 12, pp. 8230–8242, Dec. 2021.
[29] H. R. Ji, S. R. Chen, H. Yu, P. Li, J. Y. Yan, J. Y. Song, and C. S. Wang, "Robust operation for minimizing power consumption of data centers with flexible substation integration," *Energy*, vol. 248, pp. 123599, Jun. 2022.
[30] Z. S. Hou and S. T. Jin, "A novel data-driven control approach for a class of discrete-time nonlinear systems," *IEEE Transactions on Control Systems Technology*, vol. 19, no. 6, pp. 1549–1558, Nov. 2011.
[31] Y. Y. Chai, L. Guo, C. S. Wang, Z. Z. Zhao, X. F. Du, and J. Pan, "Network partition and voltage coordination control for distribution networks with high penetration of distributed PV units," *IEEE Transactions on Power Systems*, vol. 33, no. 3, pp. 3396–3407, May 2018.
[32] P. Li, H. R. Ji, C. S. Wang, J. L. Zhao, G. Y. Song, F. Ding, and J. Z. Wu, "Coordinated control method of voltage and reactive power for active distribution networks based on soft open point," *IEEE Transactions on Sustainable Energy*, vol. 8, no. 4, pp. 1430–1442, Oct. 2017.

Yanda Huo received B.S. and Ph.D. degrees in Electrical Engineering from Tianjin University, Tianjin, China, in 2016 and 2022, respectively. He is currently a Postdoc Fellow with Tianjin University. His research interests include distributed generation systems and optimal operation of distribution networks.

Peng Li received B.S. and Ph.D. degrees in Electrical Engineering from Tianjin University, Tianjin, China, in 2004 and 2010, respectively. He is currently a Professor with the School of Electrical and Information Engineering, Tianjin University. His current research interests include operation and planning of active distribution networks, modeling, and transient simulation of power systems. Prof. Li is an Associate Editor of *IEEE Transactions on Sustainable Energy*, *CSEE Journal of Power and Energy Systems*, *Sustainable Energy Technologies and Assessments*, and *IET Renewable Power Generation*.

Haoran Ji received B.S. and Ph.D. degrees in Electrical Engineering from Tianjin University, Tianjin, China, in 2014 and 2019, respectively. From 2019 to 2021, he was a Postdoctoral Research with Tianjin University. He is currently an Associate Professor in Tianjin University. His research interests include distributed generation systems and optimal operation of distribution networks. He was supported by China National Postdoctoral Program for Innovative Talents in 2019.

Hao Yu received the B.S. and Ph.D. degree in Electrical Engineering from Tianjin University, Tianjin, China, in 2010 and 2015, respectively. He is currently an Associate Professor with the School of Electrical and Information Engineering, Tianjin University. His current research interests include the operation analysis and optimization of active distribution networks and integrated energy systems. He is the assistant editor IET Energy Systems Integration.

Jinli Zhao received the Ph.D. degree in Electrical Engineering from Tianjin University, Tianjin, China, in 2007. She is currently an Associate Professor in the School of Electrical and Information Engineering, Tianjin University. Her research interests include power system security and stability.

Wei Xi received the M.S. degree in Electrical Engineering from Huazhong University of Science and Technology, Wuhan, China, in 2003. He is currently working toward the Ph.D. degree in Electrical Engineering with Tianjin University, Tianjin, China. He is currently a Professorate Senior Engineer with the Digital Power Grid Research Institute, China Southern Power Grid. His current research interests include electric power chip development and digitization of power grid.

Jianzhong Wu received the Ph.D. from Tianjin University, Tianjin, China, in 2004. From 2004 to 2006, he was at Tianjin University, where he was an Associate Professor. From 2006 to 2008, he was a Research Fellow at the University of Manchester, Manchester, U.K. He is currently a Professor with the Cardiff School of Engineering, Institute of Energy, London, U.K. His current research interests include energy infrastructure and smart grids. Prof. Wu is a member of the Institution of Engineering and Technology and the Association for Computing Machinery.

Chengshan Wang received the Ph.D. degree in Electrical Engineering from Tianjin University, Tianjin, China, in 1991. He is currently a Professor with the School of Electrical and Information Engineering, Tianjin University. Prof. Wang is a Member of Chinese Academy of Engineering. His research interests include distribution system analysis and planning, distributed generation system and microgrid. Prof. Wang is the Editor-in-Chief of *IET Energy Systems Integration*. He is the Director of the Key Laboratory of Smart Grid of Ministry of Education, Tianjin University, Tianjin, China.